

A Graph-Cut Guided ROI Segmentation Algorithm with Lightweight Deep Learning Framework for Cervical Cancer Classification

Shiny T L¹, Kumar Parasuraman²

Research Scholar, Centre for Information Technology and Engineering, Manonmaniam Sundaranar University, Abishekapatti, Tirunelveli – 627 012, Tamil Nadu, India¹

Associate Professor, Centre for Information Technology and Engineering, Manonmaniam Sundaranar University, Abishekapatti, Tirunelveli – 627 012, Tamilnadu, India²

Abstract—Cervical cancer classification has witnessed numerous advancements through deep learning methods; however, existing approaches often rely on multiple models for segmentation and classification, leading to heightened computational demands and prolonged training times. In this research, a lightweight deep learning framework for cervical cancer classification is presented. The framework comprises three primary components: a Graph-Cut Guided Region of Interest (ROI) segmentation algorithm, a streamlined DenseNet architecture, and a Multi-Class Logistic Regression classifier. The Graph-Cut Guided ROI segmentation algorithm is used to accurately isolate nuclei regions within multicellular Pap smear images. This is a lightweight algorithm that is able to achieve high segmentation accuracy with minimal computational overhead. The streamlined DenseNet architecture is used to efficiently extract salient features from the segmented images. This architecture is specifically designed to reduce feature redundancy and eliminate incongruous feature maps. The Multi-Class Logistic Regression classifier is used to classify the segmented images into different cell types and stages of cervical cancer. Experimental results show the proposed method is able to achieve high classification accuracy with minimal training time. The framework was trained and evaluated on a dataset of 963 Pap smear images. The proposed framework achieved a 98% cell type classification accuracy in precision, recall, and F1-score for classifying multi-cell Pap smear images. The training loss was also very low. The average training time was 21 minutes for different sets of training images, and the average testing time was 0.50 seconds for different sizes of testing images, which is much lower than the existing methods.

Keywords—Cervical cancer classification; deep learning; lightweight deep learning framework; graph-cut guided ROI segmentation algorithm; nuclei region isolation

I. INTRODUCTION

Cervical cancer is the fourth most common cancer among women worldwide, with a substantial impact on public health [1]. The Pap smear, a widely used screening method, involves the microscopic examination of cervical cells to detect abnormalities and enable early intervention [2], [3]. Automated classification of these cells can significantly expedite the diagnosis process and facilitate timely medical intervention. In recent times, deep learning techniques have emerged as powerful tools for medical image analysis, with numerous

methodologies proposed for cervical cancer classification. While deep learning models have demonstrated impressive performance in various medical imaging tasks, they often require extensive computational resources, intricate model architectures, and prolonged training times [4], [5], [6], [7]. Many existing approaches to cervical cancer classification utilize separate models for segmentation and classification [8], [9], [16], [20]. The paradigm of utilizing separate models for segmentation and classification exacerbates the computational demands of the overall system. The need for multiple models not only increases resource requirements but also extends the time required for model training and inference. This can hinder the integration of automated cervical cancer classification systems into clinical practice, where prompt diagnosis is crucial for effective treatment planning. Additionally, some existing approaches employ feature fusion methods to combine the outputs of separate models [10], [11], [14], [18]. While these methods attempt to leverage the strengths of different models, they can introduce further complexity and potential sources of error. Integrating outputs from multiple models requires careful consideration of weightings and fusion strategies, and may not always result in optimal performance. Moreover, many existing methods for segmenting and classifying cervical cancer cells in pap smear images are only tested with single cell images [12], [13], [14]. However, in reality, Pap smear images often contain multiple cells, which can make it more difficult to accurately segment and classify the cells.

This research endeavors to address these limitations by introducing an innovative methodology that enhances computational efficiency while maintaining robust classification accuracy. To mitigate the computational burden and accelerate the time-consuming segmentation process, a lightweight Graph-Cut Guided ROI segmentation algorithm is introduced in this research. This algorithm utilizes graph-cut techniques to effectively segment nuclei regions from multicell Pap smear images. By incorporating graph-cut guidance, this proposed approach significantly improves segmentation accuracy while maintaining computational efficiency. This innovation not only expedites the preprocessing step but also ensures that accurate nuclei regions are extracted for subsequent feature extraction. To extract the meaningful and relevant features from the segmented Pap smear images, this

research employs a lightweight DenseNet architecture. DenseNet is renowned for its ability to alleviate the vanishing gradient problem and promote feature reuse across layers. The modified DenseNet architecture is tailored to the characteristics of cervical cell images, enabling efficient feature extraction while minimizing feature redundancy. The architecture's capacity to eliminate uncorrelated feature maps further enhances computational efficiency without compromising classification accuracy. After feature extraction, the next crucial step is accurate classification. A Multi-Class Logistic Regression model is adopted for this purpose. This model is well-suited for scenarios with multiple classes, such as different stages of cervical cancer. Logistic Regression is known for its simplicity and interpretability, while still delivering commendable classification performance. Integrating this classifier into the proposed architecture preserves computational efficiency without compromising the accuracy of the classification process. The collaboration between these key components results in an integrated methodology that offers several notable advantages:

1) *Computational efficiency*: By integrating lightweight Graph-Cut Guided ROI segmentation and an efficient DenseNet architecture significantly reduces computational demands.

2) *Streamlined pipeline*: The integration of segmentation, feature extraction, and classification into a cohesive pipeline eliminates the need for multiple models, simplifying the overall process and reducing model training time.

3) *Enhanced accuracy*: The precision of the segmentation process and the efficacy of the feature extraction mechanism contribute to improved classification accuracy. Accurate segmentation ensures that only relevant regions are considered for feature extraction, while the DenseNet architecture captures essential image characteristics.

Following section of the article reviews recently developed convolutional neural network (CNN) methods for cervical cancer detection. Section II outlines the literature review. Section III presents the proposed deep learning-based framework for cervical cancer classification. Section IV discusses the experimental analysis and results. Finally, Section V the paper concludes with a summary of the key findings and implications.

II. LITERATURE REVIEW

The literature review reveals a range of approaches aimed at improving cervical cancer classification using fusion and multi-model CNNs. These methods address the challenge of accurate and efficient classification while considering the complex nature of medical image analysis. However, each approach comes with its own strengths and limitations.

Md Mamunur Rahaman et al. [14]: This research proposes the DeepCervix approach, leveraging a hybrid deep feature fusion technique. By integrating XceptionNet, ResNet50, VGG19, and VG16 models, this method addresses cervical cell classification. The fusion process occurs after preprocessing, followed by fine-tuning specific layers. However, challenges might arise in effectively combining features from diverse

models, potentially affecting performance and interpretability. Ponnusamy Sukumar et al. [15]: The study introduces an automated framework for cervical cancer classification in Pap smear images. Employing watershed segmentation for cell nucleus segmentation and a feature extraction strategy involving Local Binary Pattern, texture, GLCM, laws texture, and histogram features, the approach utilizes principal component analysis for classification. The reliance on watershed segmentation could lead to issues due to local minima and noise sensitivity. Zaid Alyafeai et al. [16]: A pipeline-based architecture is suggested, featuring two pre-trained deep models for cervix region identification and tumor classification. Through modules like ROI detection, pre-processing with data augmentation, and lightweight CNN-based feature extraction, the method strives to address segmentation and classification. However, this approach's complexity, dependence on specific pre-trained models, and potential challenges in integration. Yuexiang Li et al. [17]: This research presents a model with a key-frame feature encoding network and a feature fusion network. By encoding pre- and post-acetic acid test images using ResNet-101 and employing an interpretable graph convolution network (E-GCN) for classification, the method focuses on feature fusion. The interpretability of the graph convolution network might present difficulties in a clinical setting.

Long D. Nguyen et al. [18]: An ensemble method involving feature concatenation and deep CNNs is introduced for cervical cancer classification. Combining features from InceptionResNet-v2, Inception-v3, and ResNet152, the method seeks to enhance classification. However, the substantial ensemble of CNNs might lead to resource-intensive computations and complexity. Srishti Gautam et al. [19]: The proposed deep learning-based approach addresses detection, segmentation, and classification of nuclei in single cell Pap smear images. While the focus on feature-based segmentation and AlexNet classification through transfer learning is promising, the method's applicability to diverse nucleus types should be evaluated. Deepa. K et al. [20]: This deep learning architecture emphasizes the classification of cervical cancer using a combination of segmentation and feature extraction techniques. The use of Mask Region Based Convolutional Neural Network for segmentation and subsequent feature extraction from segmented images with GLCM, Contourlet, and Gabor filters contributes to classification using VGG networks. The intricacies of combining multiple feature extraction techniques merit investigation. Swati Shinde et al. – DeepCyto [21]: DeepCyto proposes a hybrid methodology utilizing two workflows for cervical cancer classification. Integrating feature fusion vectors from pre-trained models, this approach applies machine learning ensemble and artificial neural network methods. Challenges in computational cost and adaptability to overlapping images could limit its feasibility.

III. PROPOSED METHOD

The proposed research is a deep learning-based framework for cervical cancer classification. The framework consists of five modules: dataset, contrast enhancement, graph-cut guided ROI segmentation, image augmentation, and feature extraction using lightweight DenseNet. The dataset consists of 963 pap smear images with four distinct classes: HSIL, LSIL, NIM, and

SCC. Contrast enhancement is applied to improve nuclei visibility and aid feature extraction.

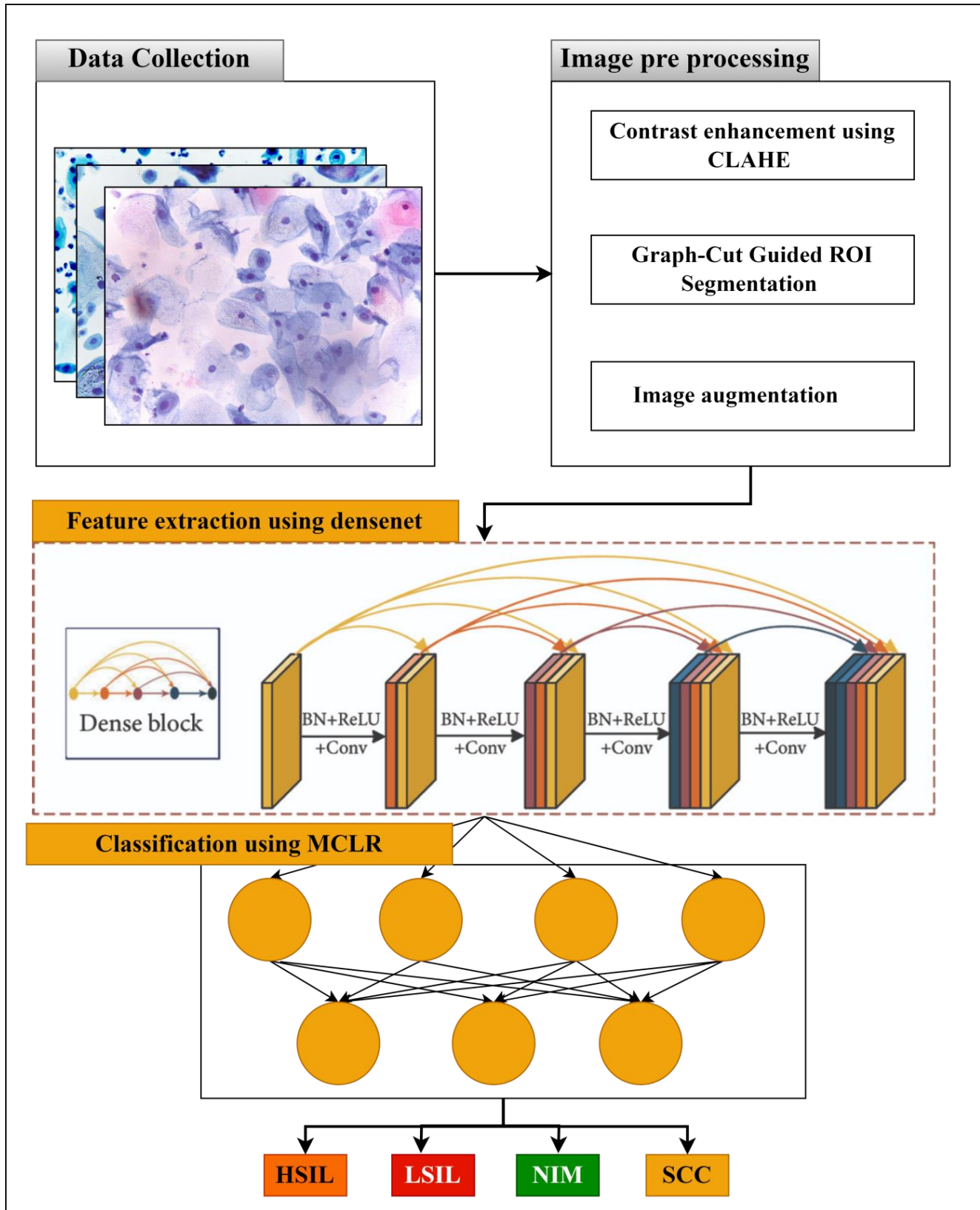


Fig. 1. Overall architecture of proposed cervical cancer classification system.

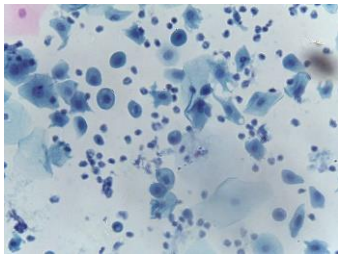
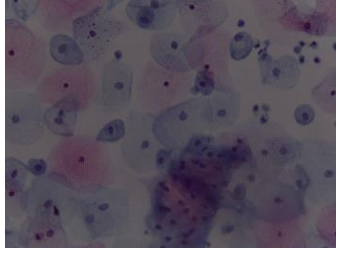
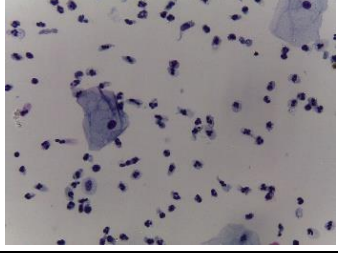
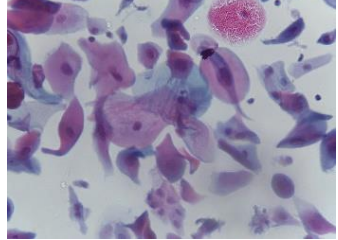
Graph-cut guided ROI segmentation is used to segment nuclei regions. Image augmentation is applied to enhance dataset diversity and generalize the deep learning model. Feature extraction using lightweight DenseNet is used to extract informative features from the segmented images. Finally, a Multi-Class Logistic Regression classifier is trained using the extracted features to classify the images into the four classes. Fig. 1 shows the overall architecture of proposed cervical cancer classification system.

A. Dataset Details

The dataset utilized in this research is named "Liquid based cytology pap smear images" [22].

This dataset was sourced from <https://data.mendeley.com/datasets/zddtpgzv63/4>, and it consists of a collection of 963 Pap smear images. These images were obtained using 40x magnification through the Leica ICC50 HD microscope. The dataset encompasses four distinct classes, each representing specific diagnostic categories. These classes are as follows: High Squamous Intraepithelial Lesion (HSIL), Low Squamous Intraepithelial Lesion (LSIL), Negative for Intraepithelial Malignancy (NIM), and Squamous Cell Carcinoma (SCC). These classes reflect different pathological conditions of cervical cells, enabling the classification of various stages of cervical cancer and cell types. Table I explains the different pap smear in the dataset.

TABLE I. DATASET OF PAP SMEAR IMAGES WITH CLASS NAMES AND NUMBER OF IMAGES

| Image name | Image | Image details | Class name | Number of images |
|--|---|---|------------|------------------|
| High Squamous Intraepithelial Lesion |  | HSIL refers to significant and advanced abnormal changes in the squamous epithelial cells of the cervix. These changes are considered more severe than low-grade lesions. HSIL is characterized by cells that appear markedly abnormal, with a higher likelihood of progressing to cervical cancer if left untreated [23]. | HSIL | 253 |
| Low Squamous Intraepithelial Lesion |  | LSIL indicates milder abnormal cellular changes in the squamous epithelial cells of the cervix. These changes are not as severe as HSIL. While LSIL is generally considered less likely to progress to cancer than HSIL, it's still important to monitor and possibly treat these cases to prevent progression. | LSIL | 198 |
| Negative for Intraepithelial Malignancy. |  | This classification indicates that the cervical cell sample appears normal and lacks any signs of intraepithelial malignancy. | NIM | 252 |
| Squamous Cell Carcinoma. |  | Squamous cell carcinoma is a type of cervical cancer that originates from the squamous epithelial cells of the cervix. This classification indicates the presence of cancerous cells within the cervical sample. It's a more advanced stage of abnormality compared to HSIL, as it indicates the presence of actively dividing and invasive cancer cells. | SCC | 260 |

B. Contrast Enhancement

Cervical cell images captured in Pap smears can have variations in intensity due to different acquisition conditions, staining procedures, and sample preparation techniques. These variations can make it challenging to differentiate between important structures like nuclei and background. Accurate nuclei detection relies on clear distinctions between nuclei and the surrounding background. Contrast enhancement enhances the visibility of nuclei, making them easier to detect. The streamlined DenseNet architecture relies on extracting meaningful features. Enhanced contrast helps the network identify subtle textures and structures, leading to more informative features. An accurate Multi-Class Logistic Regression classifier requires well-defined features. Enhanced contrast can make the differences between different cell types and stages of cervical cancer more pronounced, leading to improved classification accuracy. In this research, Contrast-Limited Adaptive Histogram Equalization (CLAHE) used to normalize the contrast of input pap smear image [24]. CLAHE enhances the contrast of an image while preventing excessive amplification of noise. It works by dividing the image into smaller regions, applying histogram equalization to each region, and then limiting the contrast amplification. The process flow of contrast enhancement is explained in Algorithm 1.

| |
|--|
| Algorithm 1. CLAHE. |
| Step 1: Divide the Image into Tiles: |
| Divide the image into tiles of size (w, h). |
| Step 2: Compute Histograms: |
| For each tile, calculate the histogram for each colour channel (R, G, and B). |
| Step 3: Histogram Equalization: |
| Apply histogram equalization to each tile's histogram to redistribute pixel intensity values and enhance local contrast. |
| The equation for histogram equalization is: |
| $f(x) = L - 1 - (L - 1) \times \frac{cdf(x)}{sum(cdf)} \quad [1]$ |

| |
|--|
| where: |
| <ul style="list-style-type: none"> • f(x) is the output intensity value for input intensity value x. • L is the number of intensity levels in the image. • cdf(x) is the cumulative distribution function of the input histogram. • sum(cdf) is the sum of the values in the input histogram. |
| Step 4: Clip Histograms: |
| To avoid over-amplification of noise, clip the histogram bins to a specified threshold. |
| The equation for clipping the histogram is: |
| $if (x > threshold) \{ x = threshold; \}$ |
| where: |
| <ul style="list-style-type: none"> • x is the current intensity value • threshold is the clipping threshold |
| Step 5: Interpolation: |
| Smooth out intensity transitions between tiles by using interpolation techniques to maintain a coherent image appearance. |
| One common interpolation technique is bilinear interpolation, which is given by the following equation: |
| $y = (x - x_0) \times (y_1 - y_2) + (x_1 - x) \times \frac{(y_0 - y_2)}{(x_1 - x_0)} \quad [2]$ |
| where: |
| <ul style="list-style-type: none"> • y is the output intensity value • x is the input intensity value • x0 and x1 are the x-coordinates of the two neighbouring pixels • y0 and y1 are the y-coordinates of the two neighbouring pixels |
| Step 6: Reconstruct the Image: |
| Merge the enhanced tiles to reconstruct the full RGB image. |

Fig. 2 illustrates the side-by-side comparison of Pap smear images before and after contrast normalization across different classes. The clear visual evidence showcases the remarkable impact of contrast enhancement using the CLAHE method. This enhancement process noticeably normalizes the contrast of the initial Pap smear images, resulting in enhanced image quality and improved visual clarity.

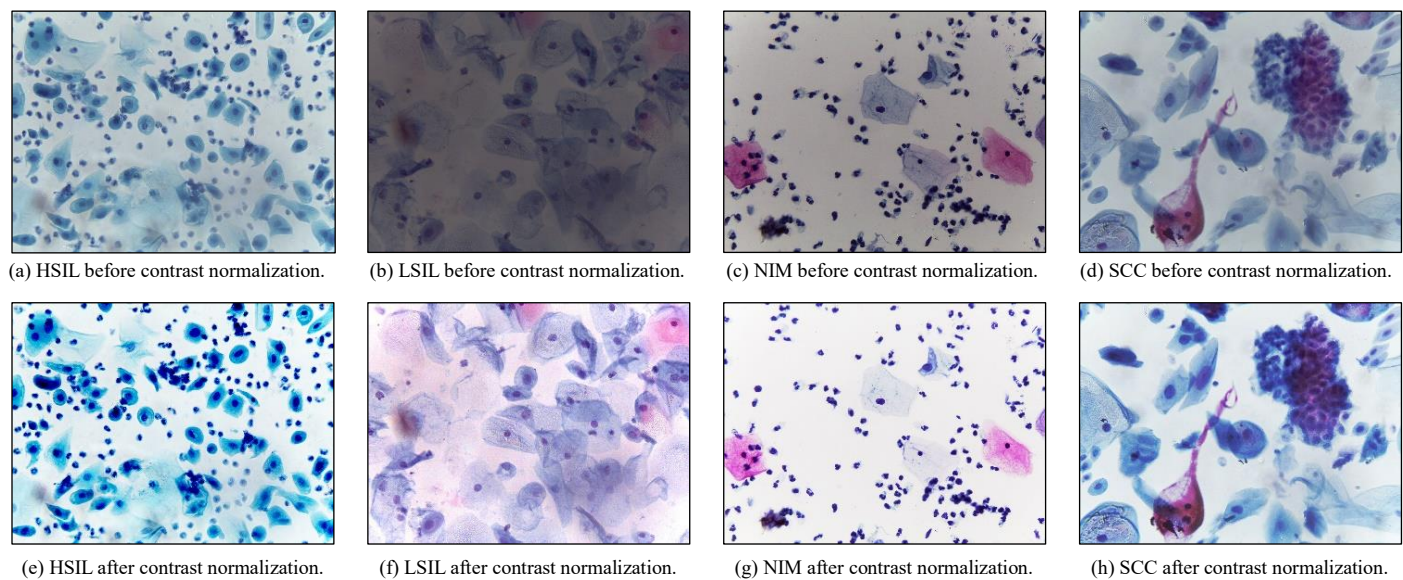


Fig. 2. Comparison of pap smear images before and after contrast normalization across different classes.

C. Proposed Graph-Cut Guided ROI Segmentation

The proposed graph-cut guided ROI segmentation algorithm is a way to divide an image into different regions of interest (ROIs). It works by using the principles of graph theory and energy minimization. By constructing a graph representation of the image, where pixels are nodes and their relationships are edges, the algorithm seeks to partition the image into foreground and background regions. Leveraging the concept of energy, the algorithm minimizes a cost function that encapsulates both local and global image characteristics. This approach yields detailed segmentation results, accurately defining nuclei regions from the complex background of multicell Pap smear images. The following steps outline the process of this segmentation method:

| |
|--|
| Algorithm. 2 graph-cut guided ROI segmentation |
| Step 1: Preprocessing |
| 1.1 Input Image Preparation: The algorithm takes an input image I consisting of multicell Pap smear data. The image is represented as a grid of pixels, where each pixel is a node in the graph. |
| Step 2: Nuclei Detection and Seed Generation |
| 2.1 Nuclei Detection: Nuclei are detected within the image I using method, S , that produces a binary mask M . |
| $M = S(I)$ [3] |
| 2.2 Seed Point Generation: For each nucleus, a seed point p_i is generated. These seed points serve as initial markers for the graph-cut segmentation process. |
| $p_i = (x_i, y_i), i = 1, 2, \dots, N$ [4] |
| Step 3: Graph Construction |
| 3.1 Construction of Graph: A graph $G = (V, E)$ is constructed, where V is the set of nodes (pixels) and E is the set of edges. Each pixel v_{ij} is a node in the graph. |
| $V = \{v_{ij}\}, i = 1, 2, \dots, H; j = 1, 2, \dots, W$ [5] |

| |
|---|
| 3.2 Edge Weights: Edge weights w_{ij} , are assigned based on pixel intensities and spatial relationships. |
| $w_{ij,kl} = \exp\left(-\frac{(i-j-k-l)^2}{2\sigma_l^2}\right) \cdot \exp\left(-d_{ij}, \frac{kl^2}{2\sigma_d^2}\right)$ [6] |
| Step 4: Graph-Cut Segmentation |
| 4.1 Energy Minimization: The energy E is minimized to find the optimal cut that separates the foreground and background regions. The energy function involves unary and pairwise terms. |
| $E = \sum_i D_i(s_i) + \sum_{i,j} V_{ij}(s_i, s_j)$ [7] |
| Where D_i is the data cost, V_{ij} is the pairwise cost, and s_i is the label of node v_{ij} . |
| 4.2 Seed Propagation: The segmented regions S obtained from the graph-cut process are refined using a seed propagation mechanism. |
| $S = SeedPropagate(M, S)$ [8] |
| Step 5: ROI Extraction |
| 5.1 Region of Interest Extraction: The segmented nuclei regions R are extracted from the input image I using the refined segmentation S . |
| $R = I \odot S$ [9] |
| Step 6: Postprocessing |
| 6.1 Noise Reduction: Postprocessing techniques such as morphological operations and noise reduction filters are applied to R to remove small artifacts. |
| $R = MorphologicalOperations(R)$ [10] |
| Step 7: Output Generation |
| 7.1 Segmentation Results: The final segmented nuclei regions R are obtained as output, representing accurate identification of nuclei within the multicell Pap smear image. |

The Fig. 3 shows the results of nuclei segmentation for four different cervical cancer grades: HSIL, LSIL, NIM, and SCC using proposed Graph-Cut Guided ROI Segmentation algorithm. The algorithm's effectiveness in accurately isolating nuclei regions within multicellular Pap smear images is demonstrated through these segmentation results.

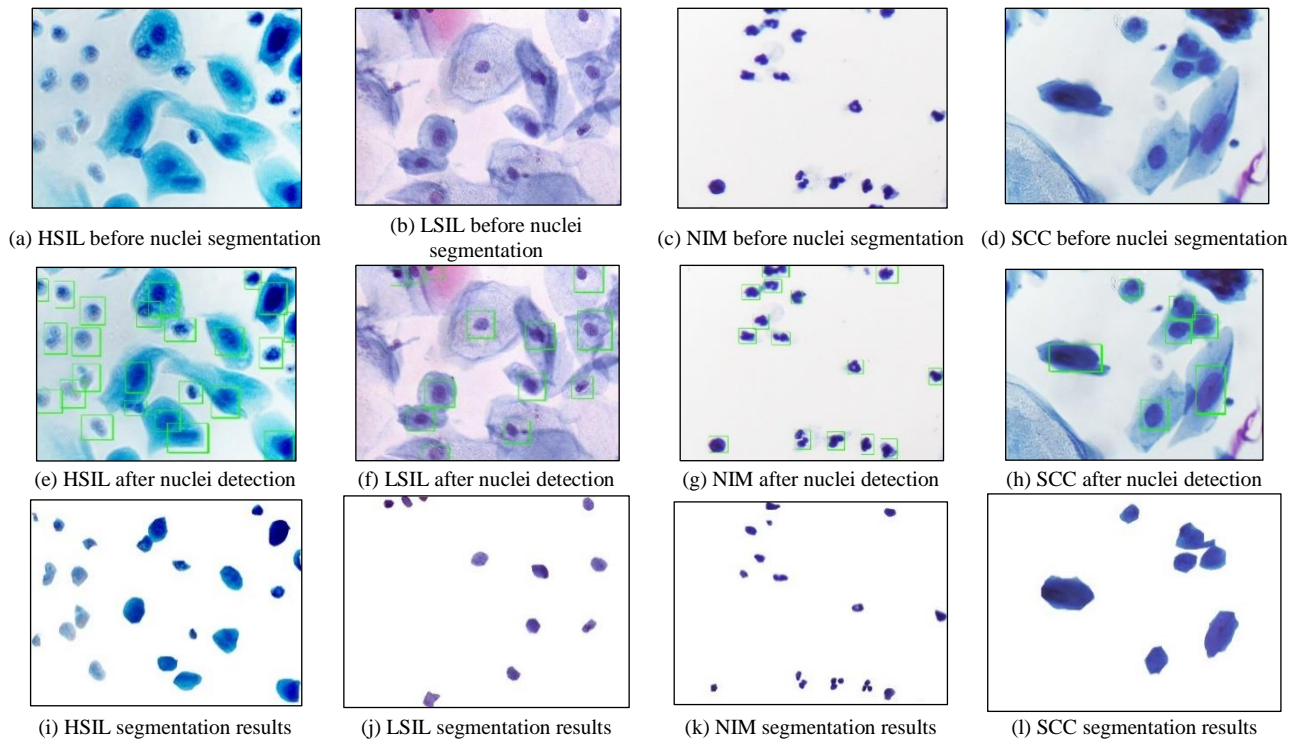


Fig. 3. Nuclei segmentation results for different cervical cancer grades using proposed Graph-Cut Guided ROI Segmentation algorithm.

D. Image Augmentation

Image augmentation is a crucial technique employed to enhance the diversity of the dataset and improve the generalization ability of the deep learning model [25]. This research, a set of image augmentation techniques is applied to the original pap smear images before being used for training. The augmentation techniques include rotation, horizontal and vertical flipping, random zooming, and brightness adjustments.

These transformations introduce variations that reflect real-world conditions and different microscope orientations, thereby minimizing the risk of overfitting and improving the model's ability to generalize to unseen data. Fig. 4 shows the different image augmentation techniques used in this research for enhanced Pap smear analysis. Data augmentation expanded the dataset from 963 to 5,778 images.

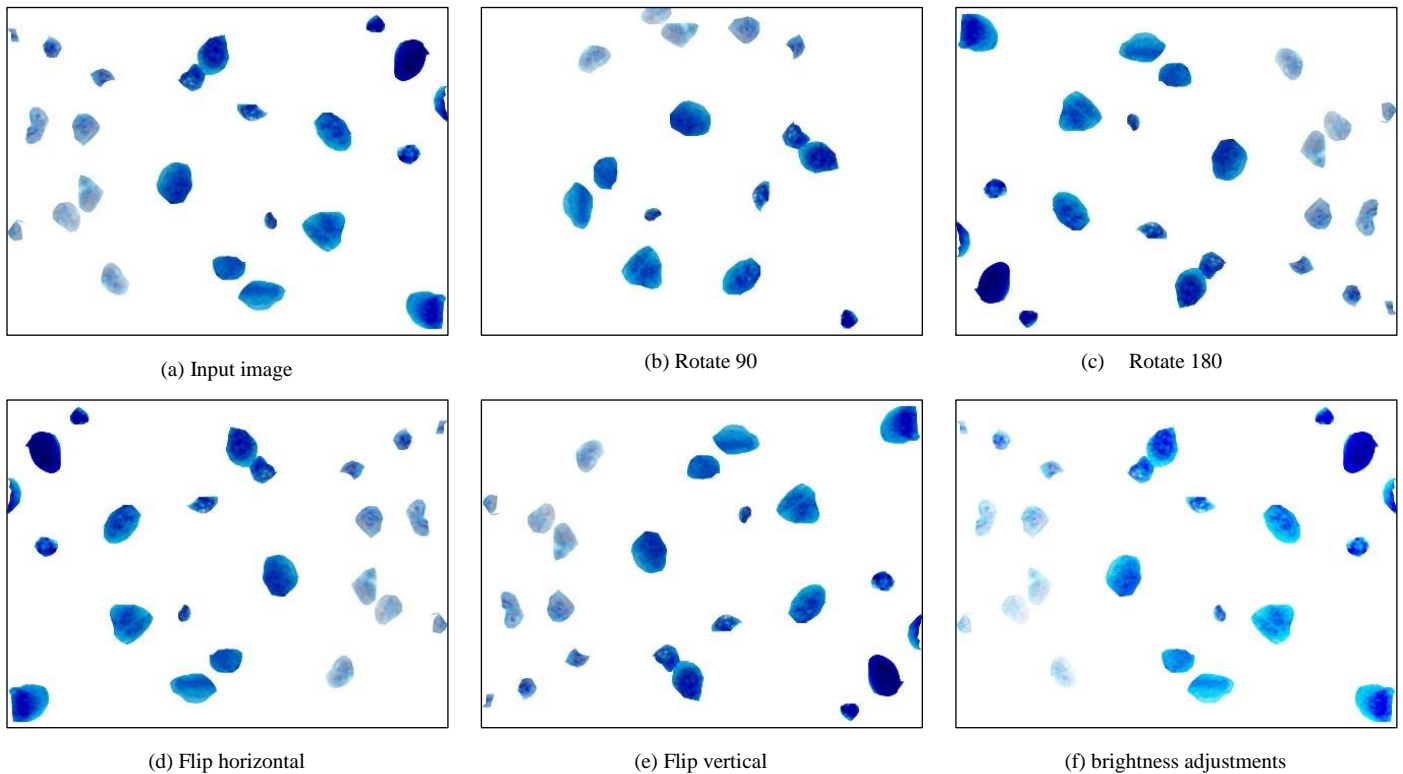


Fig. 4. Image augmentation techniques for enhanced Pap smear analysis.

E. Feature Extraction using Proposed Lightweight DenseNet

DenseNet is particularly well-suited for feature extraction from medical images due to its dense connectivity pattern [26]. Traditional convolutional architectures lose information as they progress through layers. DenseNet mitigates this by connecting each layer to every subsequent layer, ensuring that all features are directly accessible by subsequent layers [27]. This not only enhances feature propagation but also reduces the risk of information loss, making it ideal for capturing intricate structures within segmented medical images. The DenseNet architecture consists of dense blocks, each composed of multiple convolutional layers, followed by a transition layer. The key components are:

1) *Dense block*: Multiple convolutional layers are stacked together, and each layer receives the feature maps from all preceding layers. This dense connectivity encourages feature reuse and fosters information flow.

2) *Transition layer*: It follows each dense block and comprises convolutional and pooling layers. Transition layers down-sample feature maps, reducing computational load and

channel dimensions, which aids in compactly representing salient features.

To cater to the characteristics of segmented Pap smear images, a modification is introduced to the traditional DenseNet architecture. The modification's primary goals are to reduce feature redundancy and enhance feature correlation, leading to more efficient and meaningful feature extraction. In this modified DenseNet architecture, feature fusion and channel attention mechanisms are integrated within each dense block. Feature fusion combines the outputs of different convolutional layers, ensuring complementary information is considered. Channel attention recalibrates feature maps, emphasizing important channels and reducing redundancy. Table II explain the architecture details of proposed DenseNet. Fig. 5 shows the visual representation of the proposed DenseNet. The initial convolutional layer processes the input, followed by multiple dense blocks, which enhance feature extraction capabilities. Transition layers between dense blocks down-sample the feature maps, reducing computational load. The introduced modification for feature fusion and channel attention would be integrated within the dense blocks.

Specifically, the feature fusion mechanism combines features from different convolutional layers within each dense block. The channel attention mechanism recalibrates feature maps, improving feature correlation and reducing redundancy. This architecture effectively exploits the dense connectivity pattern of DenseNet, encouraging efficient feature reuse and hierarchical representation of image structures. The modification further enhances the model's ability to extract meaningful features from segmented Pap smear images, contributing to accurate cervical cancer classification.

F. Classification

The classification module of the research involves training a classifier to differentiate between different cervical cancer grades based on the features extracted from the segmented and enhanced pap smear images. A Multi-Class Logistic Regression (MCLR) classifier is employed for this purpose, leveraging the informative features obtained through the modified DenseNet architecture. The MCLR classifier assigns a probability distribution over the classes, allowing for the identification of the most likely class for each input image. Given an input feature vector \mathbf{x} , the MCLR model computes the probabilities for each class C_i using the softmax function. The probability $(C_i | \mathbf{x})$ represents the likelihood that the input \mathbf{x} belongs to class C_i . The class with the highest probability is predicted as the final output. The equation for the softmax function is:

$$(C_i | \mathbf{x}) = \frac{e^{z_i}}{\sum_{j=1}^K e^{z_j}} \tag{11}$$

TABLE II. ARCHITECTURE DETAILS OF PROPOSED DENSENET

| Layer | Type | Configuration |
|------------------------|------------------------|--|
| Input | Input | 224x224x3 (RGB with segmentation mask channel) |
| Preprocessing | Normalization | Normalize pixel values |
| Initial Convolution | Convolution | 7x7 filter, 64 filters, stride = 2, padding = 'same' |
| | Batch Normalization | |
| | ReLU Activation | |
| Dense Block | Max Pooling | 3x3 pool, stride = 2 |
| | Batch Normalization | |
| | ReLU Activation | |
| | Convolution (1x1) | k filters (bottleneck), padding = 'same' |
| | Batch Normalization | |
| Transition Layer | ReLU Activation | |
| | Convolution (1x1) | k filters (reducing channels), padding = 'same' |
| | Average Pooling | 2x2 pool, stride = 2 |
| Global Average Pooling | Global Average Pooling | Across spatial dimensions |
| Fully Connected Layers | Flatten | Flatten pooled feature maps |

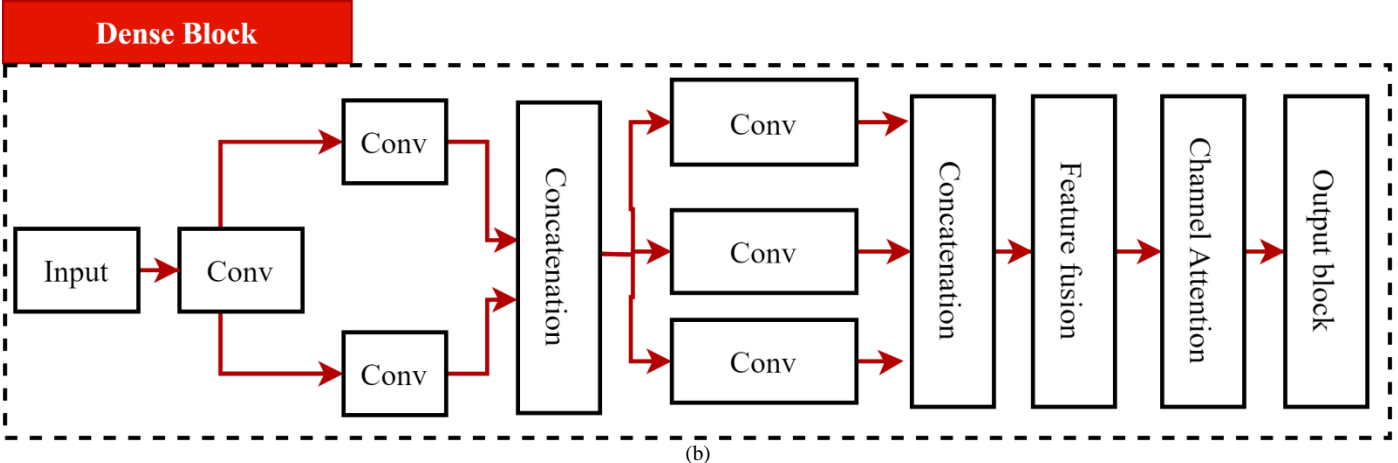
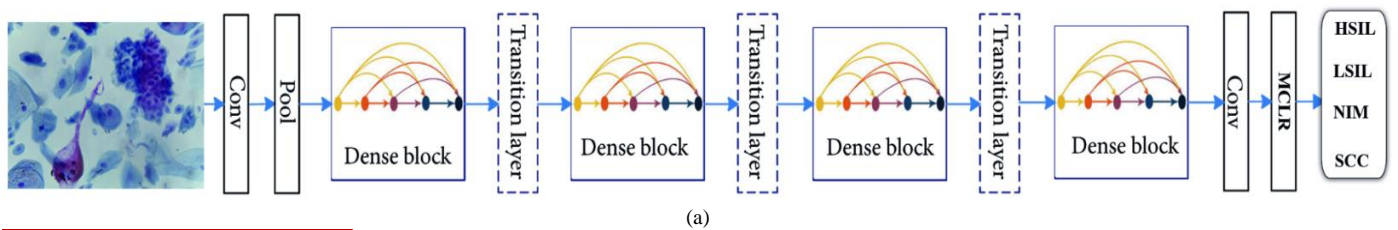


Fig. 5. Proposed DenseNet architecture (a) overall architecture (b) layer details of the proposed DenseNet block.

where: z_i is the logit for class C_i calculated as a linear combination of the feature vector \mathbf{x} and the class-specific weights. K is the total number of classes. The predicted class for an input image is the one corresponding to the highest probability among all classes. The MCLR classifier is trained using the cross-entropy loss function, it measures the dissimilarity between the predicted probabilities and the actual class labels in the training data. The formula for the Cross-Entropy Loss is as follows:

$$H(y, p) = - \sum_i y_i \log(p_i) \quad (12)$$

where: y is the ground truth label (a vector of 1s and 0s, where 1 indicates the correct class and 0 indicates the incorrect class). p is the predicted probability distribution (a vector of probabilities, where each element represents the probability of the input being in the corresponding classes: HSIL, LSIL, NIM, and SCC). i is the index of a class and \log is the natural logarithm.

IV. RESULTS AND DISCUSSION

In this section, a comprehensive analysis of the results obtained from the proposed cervical cancer detection method is presented. This section is divided into three significant parts, each contributing to a deeper understanding of the effectiveness and efficiency of the proposed approach. Firstly, the accuracy of the proposed method is evaluated in comparison to existing deep learning models and recently published cervical cancer detection systems discussed in the literature review. Specifically, a comparison is made regarding the accuracy achieved by the method against popular deep learning architectures such as AlexNet, GoogleNet, VGGNet, ResNet, and YOLO. Additionally, the method's performance is assessed against recently developed systems like the DeepCervix approach by Md Mamunur Rahaman et al. [14], utilizing a hybrid deep feature fusion technique. Furthermore, analysis is conducted on the pipeline-based architecture proposed by Alyafeai et al. [16], featuring two pre-trained deep models for cervix region identification and tumor classification. The model presented by Yuexiang Li et al. [17], which incorporates a key-frame feature encoding network and a feature fusion network, is also considered. Lastly, the deep learning architecture by Deepa. K et al. [20], emphasizing cervical cancer classification through a combination of segmentation and feature extraction techniques using two CNN models, is examined. Following this, the training efficiency of the proposed method is evaluated. Lastly, a comparison is made regarding the computational efficiency of the proposed method with existing deep learning models and recently published cervical cancer detection systems. Table III presents the parameter settings for both conventional techniques and existing deep learning models.

A. System Details

The research was conducted using a well-configured system that incorporated artificial intelligence software and hardware components. The software components included

MATLAB 2018, operating on the Windows 11 operating system. Regarding the hardware details, the system featured an Intel Core i7 processor. The system was also equipped with an NVIDIA GPU. Additionally, the system was equipped with 16GB of RAM.

B. Accuracy Analysis

Accuracy, precision, recall, and F1-measure are used to evaluate the accuracy of the proposed cervical cancer classification system. These are based on true positive cervical cancer classification (TP), true negative cervical cancer classification (TN), false positive cervical cancer classification (FP), and false negative cervical cancer classification (FN). Accuracy metrics are calculated using the following formula. The proposed cervical cancer classification system's accuracy was tested using four different types of cervical cancer cells: HSIL, LSIL, NIM, and SCC (see Section III (A)). The samples were all multicell Pap smear images.

$$Accuracy = \frac{(TP + TN)}{Total\ samples} \quad (13)$$

$$Precision = \frac{TP}{(TP + FP)} \quad (14)$$

$$Recall = \frac{TP}{(TP + FN)} \quad (15)$$

$$F1 - measure = 2 \times \frac{(Precision \times Recall)}{(Precision + Recall)} \quad (16)$$

The proposed methodology's performance is evaluated against several existing deep learning models. The comparison is presented in Tables IV, V, VI, and VII.

TABLE III. PARAMETER SETTINGS FOR CONVENTIONAL TECHNIQUES AND EXISTING DEEP LEARNING MODELS

| Parameter | Values |
|-----------------------|--------|
| Learning Rate | 0.001 |
| Batch Size | 64 |
| Activation Function | ReLU |
| Dropout Rate | 0.2 |
| Data Augmentation | Yes |
| Optimizer | Adam |
| Weight Initialization | Random |

TABLE IV. CLASSIFICATION EFFICIENCY COMPARISON FOR HSIL CELLS CLASSIFICATION WITH DEEP LEARNING MODELS

| Method | Accuracy | Precision | Recall | F1-Measure |
|-----------------|----------|-----------|--------|------------|
| AlexNet | 91.25% | 95.69% | 91.9% | 93.29% |
| GoogleNet | 93.28% | 96.70% | 92.60% | 94.60% |
| VGGNet | 94.00% | 97.20% | 93.10% | 95.10% |
| ResNet | 94.60% | 97.70% | 95.60% | 95.70% |
| YOLO | 96.72% | 97.80% | 94.60% | 95.70% |
| Proposed Method | 98.15% | 98.52% | 97.33% | 98.43% |

TABLE V. CLASSIFICATION EFFICIENCY COMPARISON FOR LSIL CLASSIFICATION WITH DEEP LEARNING MODELS

| Method | Accuracy | Precision | Recall | F1-Measure |
|-----------------|----------|-----------|--------|------------|
| AlexNet | 91.72% | 93.41% | 94.91% | 93.61% |
| GoogleNet | 92.71% | 94.91% | 94.59% | 94.78% |
| VGGNet | 93.41% | 95.40% | 95.70% | 95.20% |
| ResNet | 94.99% | 96.60% | 95.51% | 96.21% |
| YOLO | 96.10% | 95.58% | 97.59% | 97.70% |
| Proposed Method | 98.28% | 97.90% | 98.49% | 98.97% |

TABLE VI. CLASSIFICATION EFFICIENCY COMPARISON FOR NIM CLASSIFICATION WITH DEEP LEARNING MODELS

| Method | Accuracy | Precision | Recall | F1-Measure |
|-----------------|----------|-----------|--------|------------|
| AlexNet | 92.30% | 95.33% | 92.38% | 94.30% |
| GoogleNet | 93.48% | 94.91% | 93.55% | 95.10% |
| VGGNet | 91.66% | 93.43% | 92.51% | 93.91% |
| ResNet | 95.76% | 97.80% | 95.41% | 95.61% |
| YOLO | 96.81% | 98.51% | 98.69% | 91.90% |
| Proposed Method | 98.90% | 99.65% | 99.41% | 99.38% |

TABLE VII. CLASSIFICATION EFFICIENCY COMPARISON FOR SCC CLASSIFICATION WITH DEEP LEARNING MODELS

| Method | Accuracy | Precision | Recall | F1-Measure |
|-----------------|----------|-----------|--------|------------|
| AlexNet | 90.41% | 90.28% | 91.70% | 92.90% |
| GoogleNet | 93.81% | 91.83% | 90.33% | 91.80% |
| VGGNet | 91.94% | 91.48% | 92.63% | 93.18% |
| ResNet | 90.18% | 91.90% | 92.40% | 92.70% |
| YOLO | 92.30% | 93.63% | 94.64% | 94.65% |
| Proposed Method | 97.15% | 96.79% | 97.24% | 96.90% |

Table IV showcases the performance comparison of the proposed method with popular deep learning models for HSIL classification using multicell pap smear images. The accuracy of the proposed method is demonstrated to be 98.15%, which outperforms other models such as AlexNet (91.25%), GoogleNet (93.28%), VGGNet (94.00%), ResNet (94.60%), and YOLO (96.72%). Table V presents the comparison results for LSIL classification using multicell pap smear images. The proposed method again demonstrates superior performance, achieving an accuracy of 98.28%. This accuracy surpasses the other models, including AlexNet (91.72%), GoogleNet (92.71%), VGGNet (93.41%), ResNet (94.99%), and YOLO (96.10%). Table VI illustrates the comparison of NIM classification efficiency using multicell pap smear images. Once more, the proposed method stands out with an accuracy of 98.90%, outperforming AlexNet (92.30%), GoogleNet (93.48%), VGGNet (91.66%), ResNet (95.76%), and YOLO (96.81%). The comparison for SCC classification using multicell Pap smear images is presented in Table VII. The proposed method exhibits an accuracy of 97.15%, surpassing AlexNet (90.41%), GoogleNet (93.81%), VGGNet (91.94%), ResNet (90.18%), and YOLO (92.30%). Similar to previous comparisons, the proposed method achieves higher values in Precision, Recall, and F1-Measure, underscoring its effectiveness in classifying SCC using multicell pap smear

images. The analysis of the comparison tables demonstrates that the proposed methodology consistently outperforms existing deep learning models across all stages of cervical cancer classification, including HSIL, LSIL, NIM, and SCC.

C. Performance Comparison with Existing Methods

The proposed methodology addresses a critical challenge in cervical cancer classification by focusing specifically on multicell Pap smear images, where existing methods tend to show decreased accuracy. This section presents a comprehensive performance comparison between the proposed method and several existing techniques.

TABLE VIII. CLASSIFICATION EFFICIENCY COMPARISON FOR HSIL CLASSIFICATION WITH EXISTING METHODS

| Method | Accuracy | Precision | Recall | F1-Measure |
|-------------------------------|----------|-----------|--------|------------|
| Md Mamunur Rahman et al. [14] | 86.25% | 90.69% | 86.9% | 88.89% |
| Alyafeai et al. [16] | 88.28% | 91.70% | 87.60% | 89.60% |
| Yuexiang Li et al. [17] | 89.00% | 92.20% | 90.10% | 91.10% |
| Deepa. K et al. [20] | 89.60% | 93.70% | 92.60% | 92.70% |
| Proposed Method | 98.15% | 98.52% | 97.33% | 98.43% |

TABLE IX. CLASSIFICATION EFFICIENCY COMPARISON FOR LSIL CLASSIFICATION WITH EXISTING METHODS

| Method | Accuracy | Precision | Recall | F1-Measure |
|-------------------------------|----------|-----------|--------|------------|
| Md Mamunur Rahman et al. [14] | 87.13% | 90.73% | 91.36% | 90.55% |
| Alyafeai et al. [16] | 88.07% | 91.77% | 90.86% | 90.81% |
| Yuexiang Li et al. [17] | 88.73% | 92.60% | 92.90% | 92.75% |
| Deepa. K et al. [20] | 90.24% | 93.70% | 92.07% | 92.94% |
| Proposed Method | 98.28% | 97.90% | 98.49% | 98.97% |

TABLE X. CLASSIFICATION EFFICIENCY COMPARISON FOR NIM CLASSIFICATION WITH EXISTING METHODS

| Method | Accuracy | Precision | Recall | F1-Measure |
|-------------------------------|----------|-----------|--------|------------|
| Md Mamunur Rahman et al. [14] | 87.30% | 90.33% | 87.38% | 90.30% |
| Alyafeai et al. [16] | 88.98% | 91.91% | 88.95% | 91.10% |
| Yuexiang Li et al. [17] | 86.16% | 88.43% | 87.51% | 88.91% |
| Deepa. K et al. [20] | 90.76% | 92.80% | 90.41% | 91.61% |
| Proposed Method | 98.90% | 99.65% | 99.41% | 99.38% |

TABLE XI. CLASSIFICATION EFFICIENCY COMPARISON FOR SCC CLASSIFICATION WITH EXISTING METHODS

| Method | Accuracy | Precision | Recall | F1-Measure |
|-------------------------------|----------|-----------|--------|------------|
| Md Mamunur Rahman et al. [14] | 84.29% | 84.10% | 85.38% | 84.78% |
| Alyafeai et al. [16] | 88.23% | 87.34% | 87.02% | 87.18% |
| Yuexiang Li et al. [17] | 85.58% | 85.74% | 86.15% | 85.94% |
| Deepa. K et al. [20] | 84.46% | 85.68% | 85.88% | 85.78% |
| Proposed Method | 97.15% | 96.79% | 97.24% | 96.90% |

Table VIII highlights the comparison of the proposed method with existing techniques for HSIL classification. Notably, the proposed method achieves an accuracy of 98.15%, outperforming other methods such as Md Mamunur Rahaman et al. (86.25%), Alyafeai et al. (88.28%), Yuexiang Li et al. (89.00%), and Deepa K et al. (89.60%). In Table IX, the performance comparison for LSIL classification is presented. The proposed method once again achieving an accuracy of 98.28%. This accuracy significantly surpasses existing methods such as Md Mamunur Rahaman et al. (87.13%), Alyafeai et al. (88.07%), Yuexiang Li et al. (88.73%), and Deepa. K et al. (90.24%). Table X showcases the comparison results for NIM classification. The proposed method excels with an accuracy of 98.90%, surpassing Md Mamunur Rahaman et al. (87.30%), Alyafeai et al. (88.98%), Yuexiang Li et al. (86.16%), and Deepa K et al. (90.76%). The performance comparison for SCC classification is provided in Table XI. The proposed method achieves an accuracy of 97.15%, showcasing its superiority over Md Mamunur Rahaman et al. (84.29%), Alyafeai et al. (88.23%), Yuexiang Li et al. (85.58%), and Deepa K et al. (84.46%). The performance comparison clearly illustrates the proposed method's exceptional capability in addressing the limitations of existing methods, which struggle with decreased accuracy in multicell pap smear images.

The proposed method achieves remarkable accuracy, precision, recall, and F1-Measure values, indicating its robustness in accurately identifying different cell types and cancer stages using multicell Pap smear images. The existing methods were limited by their use of single pap smear images. This can be a problem because single pap smear images may not contain enough information to accurately classify the cell type or cancer stage. According to the results, the proposed method addresses this limitation by using multicell Pap smear images.

D. Training Efficiency Analysis

The training phase of deep learning models holds paramount importance in achieving accurate and robust results. To ensure optimal training, a combination of advanced training algorithms and techniques was employed. In this research, the Adam optimizer was selected as the primary algorithm for training the model. The Adam optimizer is known for its efficiency in parameter optimization and model tuning, making it well-suited for the complex and high-dimensional nature of deep learning models. To comprehensively evaluate the performance of the proposed model, a five-fold cross-validation strategy was adopted. This approach enhances the model's generalization ability by partitioning the dataset into five subsets, with four subsets utilized for training and one subset reserved for testing. The use of cross-validation mitigates the risk of overfitting and provides a robust estimate of the model's performance on unseen data. The average testing accuracy emerged as the pivotal metric to gauge the effectiveness of the proposed cervical cancer classification system. By aggregating the accuracy results from each fold, a more comprehensive and reliable measure of the model's

classification performance was obtained. The training efficiency and effectiveness of the proposed method are visually depicted in Fig. 6 to Fig. 10. These figures show the model's performance across different folds, providing insights into its consistency and stability.

E. Computational Efficiency Analysis

This section has two sections: the first section analyses the training time analysis, and the second section analyses the testing time analysis.

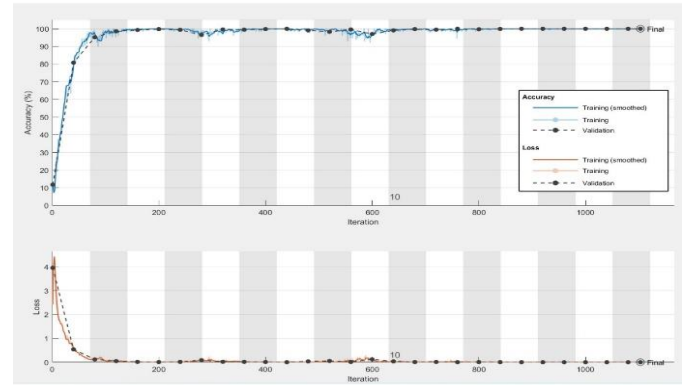


Fig. 6. Training details of cross fold 1.

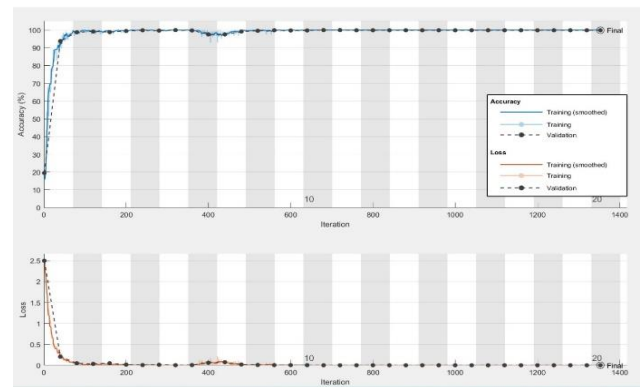


Fig. 7. Training details of cross fold 2.

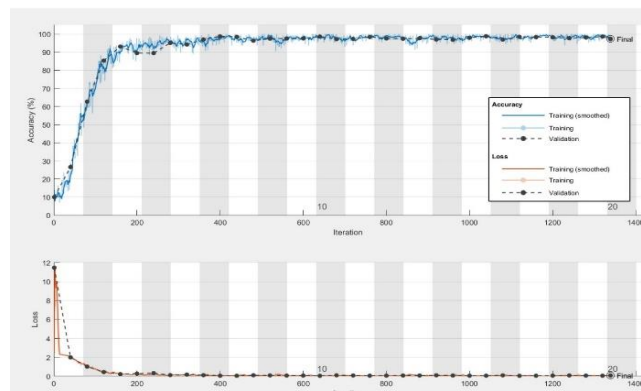


Fig. 8. Training details of cross fold 3.

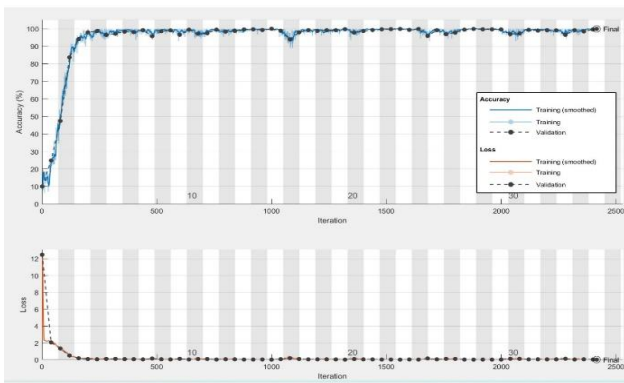


Fig. 9. Training details of cross fold 4.

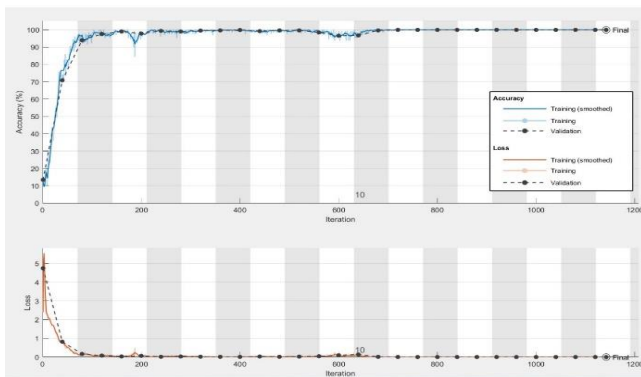


Fig. 10. Training details of cross fold 5.

The evaluation of computational efficiency plays a pivotal role in assessing the practical feasibility of deep learning models for medical image analysis. The efficiency of such models is influenced by a multitude of factors, including the effectiveness of the segmentation algorithm, the feature extraction model, the effectiveness of the training algorithm, the image type, and the image size. In order to conduct a thorough comparison of training time efficiency, three distinct sets of Pap smear images were utilized: the first set consisting of 200 images, the second containing 400 images, and the third encompassing 600 images. Each set was utilized for training the proposed deep learning model, thereby allowing for a comprehensive assessment of training time variations across different dataset sizes. The training process was carried out using the computational resources detailed in Section IV (B).

Table XII explains the training efficiency comparison results. This proposed method is much faster than existing methods. For example, it takes only 13.65 minutes to train on Dataset 1, while AlexNet, GoogleNet, VGGNet, and ResNet take 105-147 minutes. This trend continues for Dataset 2 and Dataset 3. Existing methods are effective, but they take too long to train, which is not practical for clinical applications. This proposed method is much faster without sacrificing accuracy. It uses Graph-Cut Guided ROI Segmentation and the enhanced DenseNet architecture to achieve this.

In addition to training time, the classification time of a cervical cancer classification methodology is a crucial performance metric, particularly for real-time clinical

applications. This section presents an analysis of the classification time required by various methodologies, including the proposed approach, when processing images of different sizes. The assessment is carried out using three images of varying sizes: Image 1 (800 kb), Image 2 (1200 kb), and Image 3 (1800 kb). The following table presents the classification times for each methodology when applied to the three different images.

TABLE XII. TRAINING EFFICIENCY COMPARISON RESULTS

| Methods | Dataset 1 (200 images) | Dataset 2 (400 images) | Dataset 3 (600 images) |
|---------------------------|------------------------|------------------------|------------------------|
| AlexNet | 147 minutes | 241.5 minutes | 329.25 minutes |
| GoogleNet | 131.7 minutes | 227.05 minutes | 321.8 minutes |
| VGGNet | 126 minutes | 214.6 minutes | 288 minutes |
| ResNet | 105 minutes | 171.7 minutes | 213.8 minutes |
| YOLO | 84 minutes | 154.4 minutes | 201.0 minutes |
| Md Mamunur Rahaman et al. | 60.9 minutes | 93.1 minutes | 148.7 minutes |
| Alyafeai et al. | 52.5 minutes | 81.1 minutes | 129.25 minutes |
| Yuexiang Li et al. | 63 minutes | 100.8 minutes | 135.75 minutes |
| Deepa. K et al. | 71.4 minutes | 95.25 minutes | 142.25 minutes |
| Proposed Method | 13.65 minutes | 17.85 minutes | 32.55 minutes |

This method is fast at classifying images of all sizes. For example, it takes 0.32 seconds to classify an image of 800 kb, 0.6475 seconds to classify an image of 1200 kb, and 1.04 seconds to classify an image of 1800 kb. This is important because it means that the proposed method can be used in real-time clinical applications. Other methods, such as GoogleNet, ResNet, and YOLO, are slower at classifying images of larger sizes. Alyafeai et al.'s method is fast for small images, but it becomes slower for larger images. The efficiency of proposed method is due to the Graph-Cut Guided ROI Segmentation Algorithm and the enhanced lightweight DenseNet architecture. These two techniques help to reduce the training and classification times while still ensuring accurate cervical cancer classification.

TABLE XIII. TESTING EFFICIENCY COMPARISON RESULTS

| Methods | Image 1 (800 kb) | Image 2 (1200 kb) | Image 3 (1800 kb) |
|---------------------------|------------------|-------------------|-------------------|
| AlexNet | 0.375 seconds | 0.0975 seconds | 0.4125 seconds |
| GoogleNet | 0.90 seconds | 1.80 seconds | 2.70 seconds |
| VGGNet | 0.36 seconds | 0.5475 seconds | 0.685 seconds |
| ResNet | 0.80 seconds | 1.60 seconds | 2.40 seconds |
| YOLO | 0.72 seconds | 1.32 seconds | 1.92 seconds |
| Md Mamunur Rahaman et al. | 0.0925 seconds | 0.6375 seconds | 0.975 seconds |
| Alyafeai et al. | 0.1425 seconds | 0.3475 seconds | 0.6825 seconds |
| Yuexiang Li et al. | 0.61 seconds | 1.07 seconds | 1.53 seconds |
| Deepa. K et al. | 0.67 seconds | 1.12 seconds | 1.68 seconds |
| Proposed Method | 0.32 seconds | 0.6475 seconds | 1.04 seconds |

F. Discussions

Cervical cancer is a major global health concern, and the accurate classification of cervical cells plays a critical role in its early detection and effective treatment. Many existing approaches to cervical cancer classification use separate models for segmentation and classification. This approach not only escalates computational demands but also prolongs training and inference times. The proposed method addresses this issue by integrating segmentation and classification into a single pipeline. The Graph-Cut Guided ROI Segmentation Algorithm and the enhanced lightweight DenseNet architecture enable simultaneous segmentation and feature extraction, reducing computational complexity and speeding up the overall process.

Existing approaches often rely on feature fusion to combine the outputs of separate models. However, this approach introduces complexities and potential sources of error. Proposed method avoids this pitfall by eliminating the need for feature fusion altogether. Instead, proposed unified architecture inherently incorporates both segmentation and feature extraction, mitigating the need for complicated fusion strategies. This simplification reduces the risk of errors introduced through fusion methods, leading to a more robust and accurate cervical cancer classification system.

Most existing methods for cervical cancer classification are tested with single cell images, which does not reflect the reality of pap smear images that often contain multiple cells. The proposed method directly addresses this limitation by utilizing multicell Pap smear images. The Graph-Cut Guided ROI Segmentation Algorithm effectively handles multiple cells within an image, overcoming the challenges of accurate segmentation and classification in such scenarios. This adaptability enhances the method's applicability to real-world situations, improving its reliability and clinical utility.

The results of this study demonstrate the exceptional performance of the proposed method in cervical cancer classification using multicell pap smear images. Proposed method consistently outperforms existing deep learning models and methodologies across all stages of cervical cancer classification. The accuracy, precision, recall, and F1-measure values attained underscore the method's efficacy in accurately identifying different cell types and cancer stages.

In addition, the proposed method is more efficient for training because it does not need to train multiple models or use complex feature fusion techniques. This means that it takes less time and uses fewer resources to train the model, while still being able to classify images accurately. Proposed method has been shown to be more effective than existing deep learning models for classifying cervical cancer at all stages. It is also faster and more accurate at classifying images of varying sizes. This is because proposed method uses a unified architecture that eliminates the need for complex fusion strategies.

While proposed method shows promising results, there are certain limitations that need to be acknowledged. Firstly, the performance of the method heavily relies on the quality of the input images. Variability in image quality, lighting conditions,

and staining techniques can affect the accuracy of segmentation and classification. Secondly, although proposed method improves computational efficiency compared to existing methods, there is still room for optimization to further enhance speed and resource utilization. Lastly, the evaluation of the proposed method is based on specific datasets, and its generalization to diverse populations and different acquisition conditions should be thoroughly validated before widespread clinical adoption.

V. CONCLUSION

This study presents a novel and effective approach for automated cervical cancer classification using multicell pap smear images. The method is designed to address the limitations of existing approaches and enhance the accuracy, efficiency, and practicality of cervical cancer diagnosis. The implications of these findings are profound for the medical community. This research not only highlights the potential of deep learning in transforming cervical cancer diagnosis but also addresses the critical need for efficiency in real-world applications. The successful fusion of the Graph-Cut Guided ROI Segmentation Algorithm and the enhanced lightweight DenseNet architecture demonstrates the possibility of accurate and rapid classification, even in the context of multicell pap smear images. This has the potential to enhance clinical decision-making, treatment planning, and patient outcomes.

REFERENCES

- [1] S. Pimple and G. Mishra, 'Cancer cervix: Epidemiology and disease burden', *Cytojournal*, vol. 19, no. 21, pp. 21, Mar. 2022.
- [2] Wang, C.-W., Liou, Y.-A., Lin, Y.-J., Chang, C.-C., Chu, P.-H., Lee, Y.-C., Wang, C.-H., & Chao, T.-K. (2021), "Artificial intelligence-assisted fast screening cervical high grade squamous intraepithelial lesion and squamous cell carcinoma diagnosis and treatment planning," *Scientific Reports*, vol. 11, no. 1, Aug. 2021.
- [3] K. P. Win, Y. Kitjaidure, K. Hamamoto, and T. M. Aung, "Computer-Assisted screening for cervical cancer using digital image processing of pap smear images," *Applied Sciences*, vol. 10, no. 5, p. 1800, Mar. 2020.
- [4] A. Gupta, A. Parveen, A. Kumar, and P. Yadav, 'Advancement in deep learning methods for diagnosis and prognosis of cervical cancer', *Curr. Genomics*, vol. 23, no. 4, pp. 234-245, Aug. 2022.
- [5] A. Anaya-Isaza, L. Mera-Jiménez, and M. Zequera-Diaz, "An overview of deep learning in medical imaging," *Informatics in Medicine Unlocked*, vol. 26, pp. 100723, Jan. 2021.
- [6] M. Illimoottil and D. T. Ginat, "Recent advances in deep learning and medical imaging for head and neck cancer treatment: MRI, CT, and PET scans," *Cancers*, vol. 15, no. 13, pp. 3267, Jun. 2023.
- [7] N. Youneszade, M. Marjani and C. P. Pei, "Deep Learning in Cervical Cancer Diagnosis: Architecture, Opportunities, and Open Research Challenges," in *IEEE Access*, vol. 11, pp. 6133-6149, 2023.
- [8] S. Dash, P. K. Sethy, and S. K. Behera, "Cervical transformation zone segmentation and classification based on improved inception-ResNet-V2 using colposcopy images", *Cancer Inform.*, vol. 22, pp. 1-8, Mar. 2023.
- [9] N. Nanthini, B. Kaviya Sree, M. Kavya and K. Monika, "Cervical Cancer Cell Segmentation and Classification using ML Approach," In: *Proc. of 7th International Conf. Communication and Electronics Systems (ICCES)*, Coimbatore, India, 2022, pp. 1090-1095.
- [10] H. Alquran, M. Alsaliat, W. A. Mustafa, R. A. Abdi, and A. R. Ismail, "Cervical Net: A novel cervical cancer classification using feature fusion," *Bioengineering*, vol. 9, no. 10, pp. 578, 2022.
- [11] S. Shinde, M. Kalbhor, and P. Wajire, "DeepCyto: a hybrid framework for cervical cancer classification by using deep feature fusion of

- cytology images”, *Math. Biosci. Eng.*, vol. 19, no. 7, pp. 6415–6434, Apr. 2022.
- [12] A. Ghoneim, G. Muhammad, and M. S. Hossain, “Cervical cancer classification using convolutional neural networks and extreme learning machines,” *Future Generation Computer Systems*, vol. 102, pp. 643–649, Jan. 2020.
- [13] N. Youneszade, M. Marjani and C. P. Pei, "Deep Learning in Cervical Cancer Diagnosis: Architecture, Opportunities, and Open Research Challenges," in *IEEE Access*, vol. 11, pp. 6133-6149, 2023.
- [14] Rahaman, M. M., Li, C., Yao, Y., Kulwa, F., Wu, X., Li, X., & Wang, Q, “DeepCervix: A deep learning-based framework for the classification of cervical cells using hybrid deep feature fusion techniques,” *Computers in Biology and Medicine*, vol. 136, pp. 104649, Sep. 2021.
- [15] P. Sukumar and S. Ravi, “Computer aided detection and classification of Pap smear cell images using principal component analysis”, *Int. J. Bio-inspired Comput.*, vol. 11, pp. 257, 2018.
- [16] Z. Alyafeai and L. Ghouti, "A fully-automated deep learning pipeline for cervical cancer classification," *Expert Systems with Applications*, vol. 141, pp. 112951, 2020.
- [17] C. Tang, J. Chang, C. Chu, K. Ma, Q. Li, Y. Zheng, “Computer-aided cervical cancer diagnosis using time-lapsed colposcopic images”, *IEEE Trans. Med. Imaging*, vol. 39, no. 11, pp. 3403–3415, Nov. 2020.
- [18] L. D. Nguyen, R. Gao, and D. Lin, “Biomedical image classification based on a feature concatenation and ensemble of deep CNNs”, *J Ambient Intell Human Comput*, vol. 9, no. 10, pp. 578-591, 2019.
- [19] S. Gautam, H. K. K., N. Jith, A. K. Sao, A. Bhavsar, and A. Natarajan, “Considerations for a PAP smear image analysis system with CNN features”, *arXiv [cs.CV]*, 23-Jun-2018.
- [20] K. Deepa, “PAP smear Image Classification to Predict Urinary Cancer Using Artificial Neural Networks”, *Annals of the Romanian Society for Cell Biology*, vol. 25, no. 2, pp. 1092–1098, 2021.
- [21] C. Li, H. Chen, L. Zhang, N. Xu, D. Xue, Z. Hu, H. Ma, and H. Sun, "Cervical Histopathology Image Classification Using Multilayer Hidden Conditional Random Fields and Weakly Supervised Learning," in *IEEE Access*, vol. 7, pp. 90378-90397, 2019.
- [22] E. Hussain, ‘Liquid based cytology pap smear images for multi-class diagnosis of cervical cancer’. *Mendeley*, 2019.
- [23] A. Alrajjal, V. Pansare, M. S. R. Choudhury, M. Y. A. Khan, and V. B. Shidham, ‘Squamous intraepithelial lesions (SIL: LSIL, HSIL, ASCUS, ASC-H, LSIL-H) of Uterine Cervix and Bethesda System’, *Cytojournal*, vol. 18, no. 16, pp. 16, Jul. 2021.
- [24] G. F. C. Campos, S. M. Mastelini, G. J. Aguiar, R. G. Mantovani, L. F. De Melo, and S. Barbon, “Machine learning hyperparameter selection for Contrast Limited Adaptive Histogram Equalization,” *Eurasip Journal on Image and Video Processing*, vol. 2019, no. 1, May 2019.
- [25] Shorten, C., Khoshgoftaar, T.M, “A survey on Image Data Augmentation for Deep Learning”, *J Big Data*, vol. 6, pp. 60, 2019.
- [26] Tao Zhou, XinYu Ye, HuiLing Lu, Xiaomin Zheng, Shi Qiu, and YunCan Liu, "Dense Convolutional Network and Its Application in Medical Image Analysis", *BioMed Research International*, vol. 2022, pp 22, 2022.
- [27] N. Hasan, Y. Bao, A. Shawon, and Y. Huang, “DenseNet Convolutional Neural Networks Application for predicting COVID-19 using CT Image,” *SN Computer Science*, vol. 2, no. 5, Jul. 2021.